CHINESE OPTICS LETTERS

Vol. 24, No. 2 | February 2026

Synthesized complex-frequency excitation for enhanced terahertz time-domain spectroscopy sensitivity

Zhiqiang Wu (武志强)[1], Siqi Peng (彭思齐)[1], Yuntao Wu (武云涛)[4], Xiaofei Liu (刘晓飞)[1], Min Li (李 敏)[1*], Xuru Jin (金旭如)[2**], Guifang Wang (王桂芳)[2,3***], Songlin Zhuang (庄松林)[1], and Qingqing Cheng (程庆庆)[1,2****]

[1] School of Optical-Electrical and Computer Engineering, University of Shanghai for Science and Technology, Shanghai 200093, China

[2] Department of Respiratory Diseases and Critical Medicine, Quzhou Hospital Affiliated to Wenzhou Medical University, Quzhou 324000, China

[3] Department of Respiratory Diseases and Critical Medicine, Huashan Hospital Affiliated to Fudan University, Shanghai 200040, China

[4] Anhui Polytechnic University, Wuhu 241000, China

*Corresponding author: minli1220@usst.edu.cn

**Corresponding author: wzjinxuru@163.com

***Corresponding author: wangguifang@fudan.edu.cn

****Corresponding author: qqcheng@usst.edu.cn

Received July 29, 2025 | Accepted September 19, 2025 | Posted Online December 16, 2025

Spectroscopy has become an effective detection tool in fields such as environmental monitoring, food safety, and public health. Terahertz time-domain spectroscopy (THz-TDS) is notable for its label-free and nondestructive evaluation capabilities, as well as its ability to extract material properties such as dielectric constants and absorption coefficients. However, the intrinsic damping of molecular materials significantly limits the sensitivity of THz-TDS in detecting trace molecules. In our study, we utilized a THz-TDS system to measure the terahertz spectra of water vapor molecules at varying interaction distances (d). By employing synthetic complex-frequency wave (CFW) excitation, virtual gain was introduced to counterbalance the intrinsic damping of water vapor molecules, thereby enhancing the sensitivity of terahertz detection. Experimental results show that applying synthetic CFW excitation to spectral responses containing phase information notably improves the detection sensitivity of water vapor molecules' absorption features in the terahertz range at two distinct interaction distances (d). Synthetic CFW excitation amplifies molecular vibrational fingerprint signals within the terahertz range, expanding the potential applications of THz-TDS in fields such as molecular identification, pharmaceutical analysis, and carrier dynamics in semiconductors.

Keywords: spectroscopy; complex-frequency wave; terahertz.

DOI: 10.3788/COL202624.023001

1. Introduction

The application of spectroscopic techniques spans diverse disciplines, playing a pivotal role in biomedicine[1–7], material science[8–11], and pharmaceutical research[12–15]. It aids in early diagnosis of diseases[4,5,16], the study of material properties[17–22], and the rapid detection of toxic agents[23,24]. Terahertz time-domain spectroscopy (THz-TDS), as one of the promising techniques, has garnered significant attention for its wide spectral information[25] and high temporal resolution[26]. Moreover, THz-TDS is a coherent-detection-based spectroscopic technique, enabling it to provide comprehensive spectral information about materials, including dielectric properties[27–29], absorption characteristics[30], and dynamic behaviors[12,31–35]. This capability highlights the extensive application potential of THz-TDS in fields such as material characterization[36,37], cancer detection[16], and nondestructive evaluation[38–40].

However, the intrinsic damping in molecular materials weakens the interaction between molecular vibrational modes and terahertz electromagnetic fields, posing a significant challenge for the effective detection of trace molecules. This limitation substantially restricts the broader application of THz-TDS technology across various fields. To address this issue, efforts have been made to introduce additional optical gain materials[41,42] to compensate for the intrinsic damping of molecular materials. However, optical gain materials usually increase instability and noise[43,44], which hinders the precise detection of trace molecules.

Studies have demonstrated that complex-frequency waves (CFWs) with temporal attenuation can provide virtual gain to

the system[45–52], effectively compensating for information loss caused by intrinsic system damping. A CFW with a negative imaginary part corresponds to a wave with temporal attenuation. The mathematical expression of the CFW is expressed as $E(t) \sim e^{-i\tilde{\omega}_0 t}$, where t denotes time, $\tilde{\omega}_0 = \omega_0 - i\tau/2$, and $\tau > 0$ is the temporal attenuation factor. Moreover, CFWs can avoid the additional noise and instability typically associated with optical gain materials. However, producing CFWs in real optical systems remains a challenging task, encompassing two key aspects: the need for precise CFW synthesis and time-gated measurements after reaching the quasi-steady state[53].

Recently, Zhang *et al.* resolved this challenging task through the synthesis of truncated CFW via a multi-frequency approach[53]. In their study, the CFW is regarded as a coherent combination of multiple real-frequency waves. Optical responses at real frequencies are experimentally measured and subsequently reconstructed by numerically synthesizing these responses under the framework of a Lorentzian lineshape, enabling the simulation of optical responses under complex-frequency excitation. Building on this advancement, recent works demonstrate that the introduction of virtual gain via the synthetic CFW has been effectively applied in various fields, including superlens imaging[53], polariton propagation[54], and infrared molecular sensing[55,56]. This approach has been proven to effectively compensate for intrinsic system damping, offering a powerful tool for addressing energy dissipation in these cutting-edge applications.

Here, we utilized a THz-TDS detection platform to measure the terahertz spectra of water vapor molecules at interaction distances (d) of 15 and 20 cm. Using the concept of synthetic CFW, we individually enhanced the phase-containing frequency-domain signals $\tilde{E}_S(\omega)$ and the phase-absent absorption spectra $\alpha(\omega)$. The results demonstrate that employing synthetic CFW excitation on phase-containing frequency-domain signals $\tilde{E}_S(\omega)$ effectively enhances the absorption signals within the terahertz spectra $\alpha_{\mathrm{CFW2}}(\tilde{\omega})$ of water vapor molecules at interaction distances of 15 and 20 cm. The synthetic CFW effectively promotes the interaction between molecular vibrational modes and the terahertz field, significantly enhancing THz-TDS detection sensitivity. Consequently, it establishes an approach for enhancing molecular detectability in the terahertz regime, applicable to a wide range of fields.

2. Simulation

Initially, we utilize the commercial software CST Microwave Studio to perform numerical simulations in the terahertz range, aiming to explore the efficacy of synthetic CFW in compensating for the intrinsic damping of materials. The fundamental working mechanism is illustrated in Fig. 1(a). We model molecular materials with four different damping rates based on the Drude-Lorentz dispersion:

$$\varepsilon(\omega) = 1 + \sum_n \frac{\omega_{pn}^2}{\omega_n^2 - \omega^2 - i\gamma_n\omega}. \tag{1}$$

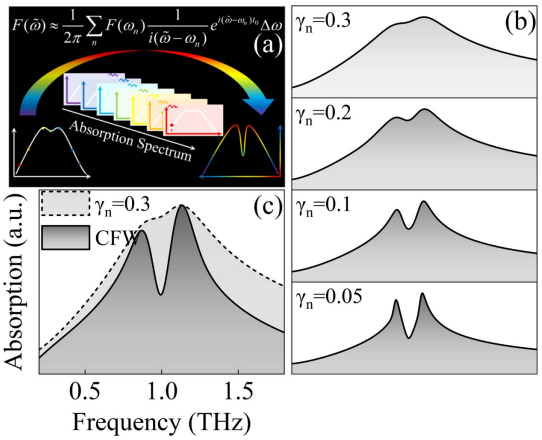

Fig. 1. Compensation of intrinsic damping in molecular materials using the synthetic CFW. (a) Schematic of intrinsic damping compensation using the synthetic CFW. (b) Simulated absorption spectra of materials with varying damping rates, based on the Drude–Lorentz dispersion model, with γ_n = 0.05, 0.1, 0.2, and 0.3 THz. (c) Absorption spectrum of material with γ_n = 0.3 THz under synthetic CFW excitation, compared with the original spectrum.

In the simulation, we assume that the molecular material has two vibrational modes, where the plasma frequencies $\omega_{p1} = \omega_{p2} = 5$ THz, the resonant frequencies $\omega_1 = 0.9$ THz and $\omega_2 = 1.1$ THz, and the damping rates are set as $\gamma_1 = \gamma_2 = 0.05$ THz for the first case, and 0.1, 0.2, and 0.3 THz for the subsequent cases. The absorption spectra of molecular materials with different damping rates are obtained through numerical simulations, as shown in Fig. 1(b).

Obviously, as the intrinsic damping γ_n increases, the interaction between molecular vibrational modes and the optical field is progressively weakened. This results in broader and less pronounced molecular absorption peaks, making detection more challenging. Consequently, reducing γ_n is advantageous for recovering distinct molecular absorption features. To compensate for intrinsic damping, synthetic CFW excitation is implemented. The response under truncated CFW excitation $E_T(t_0) = E_0 e^{-i\tilde{\omega}t_0}\theta(t_0)$ is numerically synthesized in accordance with Eq. (2) [$F(\omega_n)$ is the real-frequency response, $F(\tilde{\omega})$ is the complex-frequency response, and $\tilde{\omega} = \omega - i\gamma/2$ is the complex frequency]; t_0 denotes the time parameter in the synthesized CFW response, which corresponds to the time after the system has reached a quasi-steady state[55]. A truncated CFW can be Fourier-transformed into a Lorentzian lineshape in the frequency domain. As indicated by Eq. (2), the field under complex-frequency excitation in the time domain can be synthesized by combining measured field values at multiple real frequencies, weighted by coefficients that follow this Lorentzian lineshape. Consequently, in a linear system, any physical parameter defined at a complex frequency can be reconstructed from measurements taken at multiple real frequencies. By summing all contributions according to Eq. (2), the complex-frequency response of the system is obtained, as illustrated in Fig. 1(c):

$$F(\tilde{\omega}) \approx \sum_n F(\omega_n) \frac{1}{i(\tilde{\omega}-\omega_n)} e^{i(\tilde{\omega}-\omega_n)t_0} \Delta\omega/2\pi. \quad (2)$$

In alignment with expectations, the absorption peaks of the molecule ($\gamma_n = 0.3$ THz) are restored under synthetic CFW excitation, displaying a peak splitting comparable to that observed at $\gamma_n = 0.05$ THz. This indicates that the virtual gain provided by the synthetic CFW can substantially reduce γ_n, significantly enhancing the interaction between molecular vibrational modes and the optical field.

3. Experimental Results and Discussion

To further investigate the effectiveness of the synthetic CFW method in enhancing terahertz spectral sensitivity, we utilize a THz-TDS system to measure the terahertz spectra of water vapor molecules in air at room temperature with 35.9% relative humidity (RH), as shown in Fig. 2(a). In the experiment, the interaction distance d between the terahertz field and water vapor molecules is controlled by adjusting the central spacing between the off-axis parabolic mirrors to 15 and 20 cm. This setup enables the terahertz field to excite hydrogen bond vibrations in water vapor molecules, which are absorbed at specific resonance frequencies. The measured terahertz time-domain signals T_S of water vapor molecules, along with the reference signals T_{R1} (RH = 0.5%), are obtained by filling with high-purity nitrogen under identical conditions, as illustrated in Fig. 2. Note that accurate CFW post-processing requires sufficient frequency resolution. Achieving finer resolution requires a larger number of frequency samples, which in turn necessitates longer time-domain acquisitions. This requirement is consistent with the mathematics underlying Eq. (2). In summary, longer time-domain recordings provide higher frequency resolution and lead to more reliable CFW synthesis.

Fourier transforms are applied to the time-domain signals of both the water vapor molecules and the reference to derive the corresponding frequency-domain signals, $\tilde{E}_S(\omega)$ for the water vapor molecules and $\tilde{E}_{R1}(\omega)$ for the reference. The information-rich frequency band (0.2–2.3 THz) is subsequently selected to extract the relevant frequency-domain spectra, as illustrated in Fig. 3.

Next, the absorption spectra $\alpha(\omega)$ of water vapor molecules within the target frequency band are obtained by Eq. (3) (t_{12} and t_{21} denote the amplitude transmission coefficients for the terahertz wave at the sample cell interface during "incidence" and "exit," respectively; in this study, $t_{12} \approx t_{21} \approx 1$), as illustrated in Figs. 4(a) and 4(b):

$$\alpha(\omega) = \frac{1}{d} \log\left(\frac{\mathrm{abs}(\tilde{E}_S(\omega)/\tilde{E}_R(\omega))}{t_{12}t_{21}}\right). \quad (3)$$

Based on Figs. 4(a) and 4(b), at an interaction distance of $d = 20$ cm, water vapor molecules exhibit prominent absorption peaks at 1.098, 1.164, 1.412, 1.671, 1.718, 1.869, 1.921, 2.166, 2.198, 2.223, and 2.266 THz. In contrast, weaker absorption

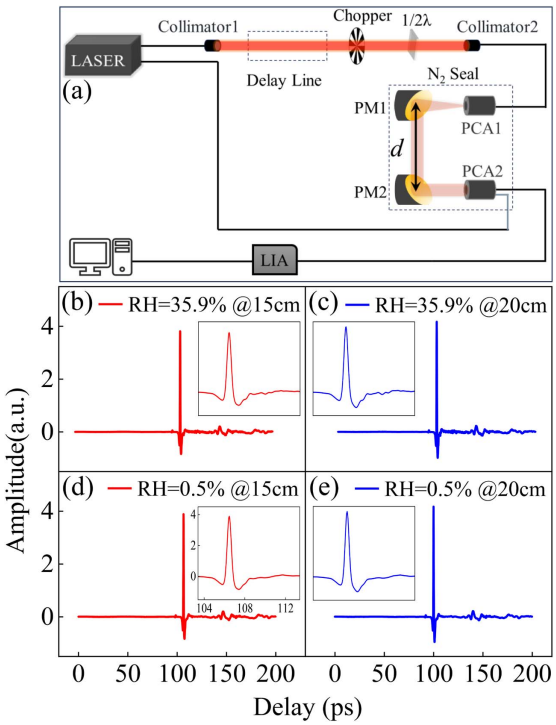

Fig. 2. THz-TDS signals. (a) Schematic of the optical path of the THz-TDS detection system. (b), (c) Time-domain signals of water vapor molecules recorded at interaction distances $d = 15$ and 20 cm, respectively, serving as sample signals. (d), (e) Corresponding reference time-domain signals measured with high-purity nitrogen at identical interaction distances, $d = 15$ and 20 cm. The insets show an amplified segment of the respective time-domain pulse.

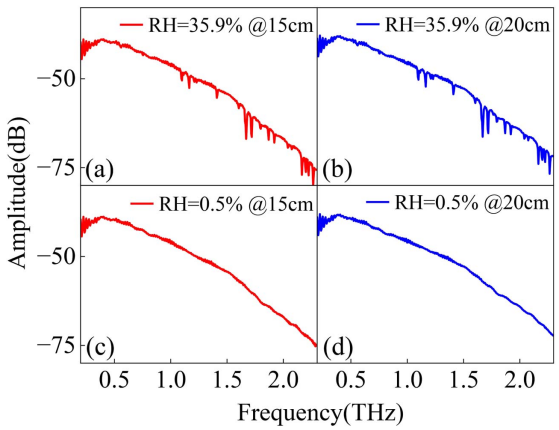

Fig. 3. THz-TDS frequency-domain signals. (a), (b) Frequency-domain spectra obtained by performing Fourier transforms on the time-domain signals of water vapor molecules at interaction distances of $d = 15$ and 20 cm, respectively. (c), (d) Corresponding frequency-domain spectra derived from Fourier transforms of the reference time-domain signals under identical conditions at $d = 15$ and 20 cm.

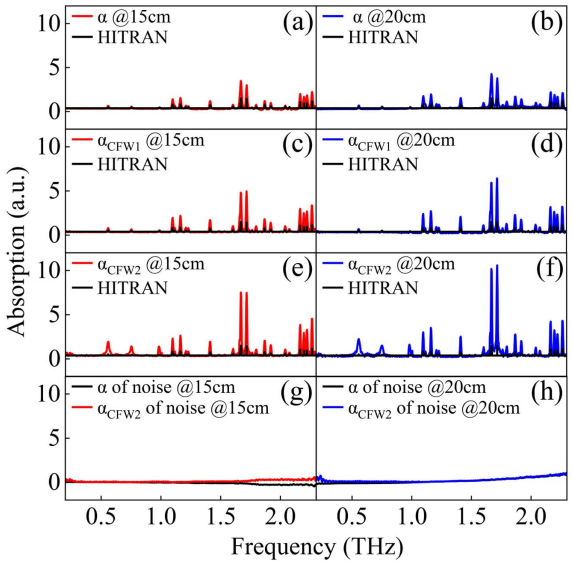

Fig. 4. Absorption spectra of water vapor molecules and the noise. (a), (b) Absorption spectra, $\alpha(\omega)$, calculated using Eq. (3) at interaction distances of 15 and 20 cm, respectively, compared with the HITRAN standard spectrum. (c), (d) $\alpha(\omega)$ under CFW excitation, denoted as $\alpha_{CFW1}(\tilde{\omega})$, at interaction distances of 15 and 20 cm, respectively, compared with the HITRAN standard spectrum. (e), (f) Absorption spectra, $\alpha_{CFW2}(\tilde{\omega})$, obtained by applying CFW excitation to $\tilde{E}_S(\omega)$ (resulting in $\tilde{E}_{SCFW}(\tilde{\omega})$), followed by the calculation through Eq. (3) at interaction distances of 15 and 20 cm, respectively, compared with the HITRAN standard spectrum. (g), (h) Comparison of the real-frequency and complex-frequency absorption spectra of the noise at interaction distances of 15 and 20 cm, respectively.

peaks are observed at 0.557, 0.753, 0.989, 1.208, 1.229, 1.603, 1.763, 1.796, 2.042, and 2.076 THz. When the interaction distance between the terahertz field and water vapor molecules is reduced to $d = 15$ cm, all 21 absorption peaks of water vapor molecules are attenuated to varying degrees. Notably, the peaks at 0.557, 0.753, and 0.989 THz become increasingly faint and are almost indistinguishable from noise. When the interaction distance d decreases, the intrinsic damping of water vapor molecules more prominently attenuates the interaction between their vibrational modes and the terahertz field. Consequently, at very low molecular concentrations, the molecular spectral signals become substantially diminished and broadened, ultimately being overwhelmed by background noise.

To introduce virtual gain to compensate for the intrinsic damping of water vapor molecules, the complex-frequency response $\alpha_{CFW1}(\tilde{\omega})$ of $\alpha(\omega)$, under synthetic CFW excitation, is synthesized based on Eq. (2), as illustrated in Figs. 4(c) and 4(d). Compared to the original absorption spectra $\alpha(\omega)$, the complex-frequency absorption spectra $\alpha_{CFW1}(\tilde{\omega})$ exhibit no significant enhancement in absorption peaks. This result indicates that directly applying synthetic CFW excitation to $\alpha(\omega)$ does not effectively introduce virtual gain to compensate for the intrinsic damping of water vapor molecules. The lack of enhancement arises because the original absorption spectra $\alpha(\omega)$ inherently lack phase information.

Effective introduction of virtual gain to compensate for intrinsic damping is achieved by applying synthetic CFW excitation to the phase-containing frequency-domain signal $\tilde{E}_S(\omega)$. The complex-frequency-domain response of water vapor molecules under synthetic CFW excitation, $\tilde{E}_{SCFW}(\tilde{\omega})$, is synthesized based on Eq. (2). Similarly, the information-rich frequency band is selected, and the corresponding spectra are extracted. The absorption spectra $\alpha_{CFW2}(\tilde{\omega})$ under synthetic CFW excitation are obtained based on Eq. (3) and compared to the HITRAN[57] (High-Resolution Transmission Molecular Absorption Database) standard spectrum, as illustrated in Figs. 4(e) and 4(f). It is evident that synthetic CFW excitation markedly enhances the absorption peaks in the complex-frequency absorption spectra $\alpha_{CFW2}(\tilde{\omega})$, substantially improving spectral sensitivity. Additionally, the positions of absorption peaks in $\alpha_{CFW2}(\tilde{\omega})$ demonstrate excellent alignment with the HITRAN data, indicating that applying synthetic CFW excitation to the phase-containing signal $\tilde{E}_S(\omega)$ effectively introduces virtual gain to compensate for intrinsic damping.

It is noted that the complex-frequency absorption spectra $\alpha_{CFW2}(\tilde{\omega})$ exhibit fluctuations compared to the real-frequency-excited absorption spectra $\alpha(\omega)$, which originate from the sidebands induced by truncation of the CFW. The influence of these sidebands can be minimized through time-averaging. Additionally, in actual calculations, the finite frequency range and discretized frequency sampling points also contribute to a certain level of error. Specifically, during the temporal decay of the amplitude, the impact of the finite frequency range becomes increasingly pronounced, thereby increasing the instability of the synthesized CFW. Therefore, expanding the frequency range and reducing the frequency interval can effectively suppress oscillation errors and prolong the quasi-steady-state duration[53,55].

We substitute the water molecular signal with the reference signal T_{R2} (second set of reference signals, RH = 0.7%) in Eq. (3) and apply identical processing steps to obtain the real-frequency absorption spectra of the noise, in order to effectively evaluate the enhancement of terahertz spectral sensitivity by the synthesized CFW. Under the same synthesized CFW excitation conditions, the complex-frequency absorption spectra of the noise are subsequently derived. As shown in Figs. 4(g) and 4(h), the synthesized CFW induces negligible enhancement of the background noise. This is attributed to the absence of coupling between the noise and the terahertz field, which prevents the virtual gain introduced by the synthesized CFW from amplifying the noise.

To clarify that the synthesized CFW predominantly enhances the characteristic peaks of water vapor molecules, we perform differentiation on both the complex-frequency spectra $\alpha_{CFW2}(\tilde{\omega})$ and real-frequency absorption spectra $\alpha(\omega)$, extracting their differential difference, as shown in Fig. 5. It is evident that at $d = 20$ cm, the enhancement of water absorption peaks by the synthesized CFW significantly surpasses that of the noise.

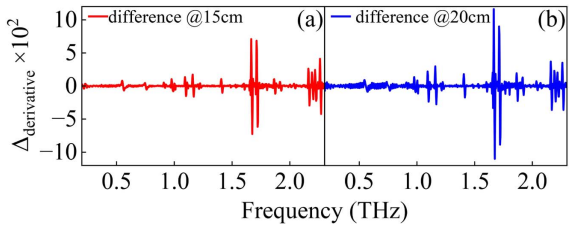

Fig. 5. Differential analysis of synthesized CFW-enhanced absorption spectra. (a), (b) Differential difference between the complex-frequency spectra $\alpha_{CFW2}(\tilde{\omega})$ and real-frequency absorption spectra $\alpha(\omega)$ at interaction distances of 15 and 20 cm, respectively

Even when the interaction distance d decreases, the synthesized CFW maintains its capability to introduce virtual gain, thereby markedly amplifying the characteristic molecular peaks of water. This mechanism effectively elevates terahertz spectral sensitivity.

Further, to evaluate the enhancement in THz-TDS spectral sensitivity enabled by the synthetic CFW, the peak heights, Δh, of the aforementioned 21 characteristic peaks are extracted from the absorption spectra $\alpha(\omega)$, $\alpha_{CFW1}(\tilde{\omega})$, and $\alpha_{CFW2}(\tilde{\omega})$. These peaks are sequentially labeled from 1 to 21, as illustrated in Fig. 6. It is observed that at both interaction distances $d = 15$ and 20 cm, the originally weak absorption peaks at 0.557, 0.753, 0.989, 1.208, 1.229, 1.603, 1.763, 1.796, 2.042, and 2.076 THz are effectively enhanced. Furthermore, even the initially more pronounced absorption peaks at 1.098, 1.164, 1.412, 1.671, 1.718, 1.869, 1.921, 2.166, 2.198, 2.223, and 2.266 THz exhibit substantial amplification. Moreover, the enhancement in sensitivity achieved by the synthetic CFW is markedly more pronounced for the phase-containing absorption spectra $\alpha_{CFW2}(\tilde{\omega})$ than for the phase-absent spectra $\alpha_{CFW1}(\tilde{\omega})$. Therefore, to ensure that

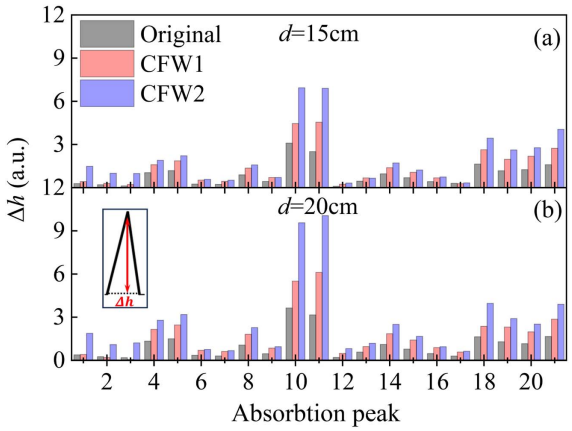

Fig. 6. Heights of absorption peaks. (a) At an interaction distance of d = 15 cm, the heights of the absorption peaks in the spectra $\alpha(\omega)$, $\alpha_{CFW1}(\tilde{\omega})$, and $\alpha_{CFW2}(\tilde{\omega})$ located at 0.557, 0.753, 0.989, 1.098, 1.164, 1.208, 1.229, 1.412, 1.603, 1.671, 1.718, 1.763, 1.796, 1.869, 1.921, 2.042, 2.076, 2.166, 2.198, 2.223, and 2.266 THz, respectively numbered from 1 to 21. (b) At an interaction distance of d = 20 cm, the heights of the 21 characteristic absorption peaks in the spectra $\alpha(\omega)$, $\alpha_{CFW1}(\tilde{\omega})$, and $\alpha_{CFW2}(\tilde{\omega})$, sequentially labeled from 1 to 21.

the virtual gain provided by the synthetic CFW effectively compensates for intrinsic damping, it is imperative to incorporate phase information within the real-frequency response.

4. Conclusion

In our study, THz-TDS is employed to measure and extract the terahertz absorption spectra of water vapor molecules at varying interaction distances d. By implementing the synthetic truncated CFW method, virtual gain is introduced to compensate for the intrinsic damping of water vapor molecules, markedly amplifying their vibrational fingerprint signals. Our approach achieves a substantial enhancement in the sensitivity of terahertz spectroscopy. Notably, incorporating phase information into the real-frequency response is essential for effectively introducing virtual gain. In conclusion, the synthetic CFW method markedly amplifies molecular signature signals, substantially elevating the sensitivity threshold of THz-TDS. The synthetic CFW method provides a highly promising platform in spectroscopy, capable of substantially enhancing sensitivity in complex environments and establishing a foundation for advancements in environmental monitoring, medical diagnostics, and material development.

Acknowledgements

Sincere thanks to Dr. Guan Fuxin for providing valuable assistance in completing this research. This work was supported by the Innovation Program for Quantum Science and Technology (No. 2023ZD0301000), the National Natural Science Foundation of China (Nos. 12174260, 12574326, and 62375173), and the Shanghai Municipal Health Commission, Clinical Research Special Program for the Health Industry (No. 202040438).

References

1. M. Brucherseifer, M. Nagel, P. Bolivar, *et al.*, "Label-free probing of the binding state of DNA by time-domain terahertz sensing," Appl. Phys. Lett. **77**, 4049 (2000).
2. S. Nakajima, H. Hoshina, M. Yamashita, *et al.*, "Terahertz imaging diagnostics of cancer tissues with a chemometrics technique," Appl. Phys. Lett. **90**, 1102 (2007).
3. P. Ashworth, E. Pickwell-MacPherson, E. Provenzano, *et al.*, "Terahertz pulsed spectroscopy of freshly excised human breast cancer," Opt. Express **17**, 12444 (2009).
4. S. Oh, J. Kang, I. Maeng, *et al.*, "Nanoparticle-enabled terahertz imaging for cancer diagnosis," Opt. Express **17**, 3469 (2009).
5. H. Cheon, H. Yang, S. Lee, *et al.*, "Terahertz molecular resonance of cancer DNA," Sci. Rep. **6**, 37103 (2016).
6. W. Chen, Y. Peng, X. Jiang, *et al.*, "Isomers identification of 2-hydroxyglutarate acid disodium salt (2HG) by terahertz time-domain spectroscopy," Sci. Rep. **7**, 12166 (2017).
7. L. Masini, S. Meucci, J. Xu, *et al.*, "Terahertz probe of individual subwavelength objects in a water environment," Laser Photonics Rev. **8**, 734 (2014).
8. M. Gaberšček, "Understanding Li-based battery materials via electrochemical impedance spectroscopy," Nat. Commun. **12**, 6513 (2021).

9. E. Kautz, A. Devaraj, D. Senor, *et al.*, "Hydrogen isotopic analysis of nuclear reactor materials using ultrafast laser-induced breakdown spectroscopy," Opt. Express **29**, 4936 (2021).
10. W. He, S. Wan, Y. Zuo, *et al.*, "Loss-enabled chirality inversion in terahertz metasurfaces," Phys. Rev. Lett. **134**, 106901 (2025).
11. X. Liu, J. Cui, C. Feng, *et al.*, "Differential photoacoustic cell-based Fourier transform photoacoustic spectroscopy for background-free gas detection," Chin. Opt. Lett. **22**, 101203 (2024).
12. P. Bawuah and J. Zeitler, "Advances in terahertz time-domain spectroscopy of pharmaceutical solids: a review," Trac-Trend Anal. Chem. **139**, 116272 (2021).
13. K. Shah, M. Shah, S. Solanki, *et al.*, "Recent advancements and applications of Raman spectroscopy in pharmaceutical analysis," J. Mol. Struct. **1278**, 134914 (2023).
14. Y. Song, Y. Cong, B. Wang, *et al.*, "Applications of Fourier transform infrared spectroscopy to pharmaceutical preparations," Expert Opin. Drug Del. **17**, 551 (2020).
15. M. Li, W. Xu, and Y. Su, "Solid-state NMR spectroscopy in pharmaceutical sciences," Trac-trend Anal. Chem. **135**, 116152 (2021).
16. J. Lou, Y. Jiao, R. Yang, *et al.*, "Calibration-free, high-precision, and robust terahertz ultrafast metasurfaces for monitoring gastric cancers," Proc. Natl. Acad. Sci. USA **119**, e2209218119 (2022).
17. L. Beardslee, M. Remillieux, and T. Ulrich, "Determining material properties of components with complex shapes using resonant ultrasound spectroscopy," Appl. Acoust. **178**, 108014 (2021).
18. J. Sunil, C. Narayana, G. Kumari, *et al.*, "Raman spectroscopy, an ideal tool for studying the physical properties and applications of metal–organic frameworks (MOFs)," Chem. Soc. Rev. **52**, 3397 (2023).
19. Z. Ren, Y. Hu, W. He, *et al.*, "Overcoming high-quality limitations in plasmonic metasurfaces for ultrasensitive terahertz applications," ACS Nano **18**, 21211 (2024).
20. B. Liu, Y. Peng, Z. Jin, *et al.*, "Terahertz ultrasensitive biosensor based on wide-area and intense light-matter interaction supported by QBIC," Chem. Eng. J **462**, 142347 (2023).
21. P. Ren, J. Zheng, Z. Huang, *et al.*, "Far-field excitation of a photonic flat band via a tailored anapole mode," Phys. Rev. Lett. **135**, 083803 (2025).
22. Z. Wu, J. Gao, Q. Yang, *et al.*, "Exploring coupling flip mechanisms via plasmon-induced transparency in active metamaterials," Chin. Opt. Lett. **23**, 023606 (2025).
23. X. Jin, Z. Xu, M. Zhang, *et al.*, "Potential toxic effects of perfluorobutanesulfonyl fluoride analysis based on multiple-spectroscopy techniques and molecular modelling analysis," Spectrochim. Acta A **308**, 123677 (2024).
24. E. Bozorgzadeh, A. Pasdaran, and H. Ebrahimi-Najafabadi, "Determination of toxic heavy metals in fish samples using dispersive micro solid phase extraction combined with inductively coupled plasma optical emission spectroscopy," Food Chem. **346**, 128916 (2021).
25. Q. Wang, L. Xie, and Y. Ying, "Overview of imaging methods based on terahertz time-domain spectroscopy," Appl. Spectrosc. Rev. **57**, 249 (2022).
26. V. Jelic, S. Adams, M. Hassan, *et al.*, "Atomic-scale terahertz time-domain spectroscopy," Nat. Photonics **18**, 898 (2024).
27. K. Hashimoto, P. Ben Ishai, E. Bründermann, *et al.*, "Dielectric property measurement of human sweat using attenuated total reflection terahertz time domain spectroscopy," Biomed. Opt. Express **13**, 4572 (2022).
28. T. Fujii, A. Ando, and Y. Sakabe, "Characterization of dielectric properties of oxide materials in frequency range from GHz to THz," J. Eur. Ceram. Soc. **26**, 1857 (2006).
29. E. Nguema, V. Vigneras, J. Miane, *et al.*, "Dielectric properties of conducting polyaniline films by THz time-domain spectroscopy," Eur. Polym. J. **44**, 124 (2008).
30. H. Wang, Y. Horikawa, S. Tsuchikawa, *et al.*, "Terahertz time-domain spectroscopy as a novel tool for crystallographic analysis in cellulose," Cellulose **27**, 9767 (2020).
31. X. Zhang, A. Shkurinov, and Y. Zhang, "Extreme terahertz science," Nat. Photonics **11**, 16 (2017).
32. T. Kampfrath, K. Tanaka, and K. Nelson, "Resonant and nonresonant control over matter and light by intense terahertz transients," Nat. Photonics **7**, 680 (2013).
33. H. Zhao, Y. Tan, L. Zhang, *et al.*, "Ultrafast hydrogen bond dynamics of liquid water revealed by terahertz-induced transient birefringence," Light Sci. Appl. **9**, 136 (2020).
34. J. Zhang, Y. Yan, L. Liu, *et al.*, "Terahertz spectroscopy of water in nonionic reverse micelles," Chin. Opt. Lett. **22**, 013001 (2024).
35. X. Cao, F. Wang, L. Xing, *et al.*, "High-resolution temporal overlap with proper dispersion compensation for a coherent photocurrent experiment revealed by terahertz time-domain emission spectroscopy," Chin. Opt. Lett. **22**, 113701 (2024).
36. H. Cheng, H. Huang, M. Yang, *et al.*, "Characterization of the remediation of chromium ion contamination with bentonite by terahertz time-domain spectroscopy," Sci. Rep. **12**, 11149 (2022).
37. D. Pashnev, T. Kaplas, V. Korotyeyev, *et al.*, "Terahertz time-domain spectroscopy of two-dimensional plasmons in AlGaN/GaN heterostructures," Appl. Phys. Lett. **117**, 1105 (2020).
38. Y. Peng, C. Shi, Y. Zhu, *et al.*, "Terahertz spectroscopy in biomedical field: a review on signal-to-noise ratio improvement," PhotoniX **1**, 1 (2020).
39. M. Tonouchi, "Cutting-edge terahertz technology," Nat. Photonics **1**, 97 (2007).
40. S. Unnikrishnakurup, J. Dash, S. Ray, *et al.*, "Nondestructive evaluation of thermal barrier coating thickness degradation using pulsed IR thermography and THz-TDS measurements: A comparative study," NDT E Int. **116**, 102367 (2020).
41. A. Fang, T. Koschny, M. Wegener, *et al.*, "Self-consistent calculation of metamaterials with gain," Phys. Rev. B **79**, 241104 (2009).
42. J. Grgić, J. Ott, F. Wang, *et al.*, "Fundamental limitations to gain enhancement in periodic media and waveguides," Phys. Rev. Lett. **108**, 183903 (2012).
43. M. Stockman, "Spaser action, loss compensation, and stability in plasmonic systems with gain," Phys. Rev. Lett. **106**, 156802 (2011).
44. J. B. Pendry and S. A. Maier, "Comment on "Spaser action, loss compensation, and stability in plasmonic systems with gain";," Phys. Rev. Lett. **107**, 259703 (2011).
45. S. Kim, Y. Peng, S. Yves, *et al.*, "Loss compensation and superresolution in metamaterials with excitations at complex frequencies," Phys. Rev. X **13**, 041024 (2023).
46. J. Hinney, S. Kim, G. Flatt, *et al.*, "Efficient excitation and control of integrated photonic circuits with virtual critical coupling," Nat. Commun. **15**, 2741 (2024).
47. A. Archambault, M. Besbes, and J. Greffet, "Superlens in the time domain," Phys. Rev. Lett. **109**, 097405 (2012).
48. D. Baranov, A. Krasnok, and A. Alù, "Coherent virtual absorption based on complex zero excitation for ideal light capturing," Optica **4**, 1457 (2017).
49. H. Li, A. Mekawy, A. Krasnok, *et al.*, "Virtual parity-time symmetry," Phys. Rev. Lett. **124**, 193901 (2020).
50. H. Tetikol and M. Aksun, "Enhancement of resolution and propagation length by sources with temporal decay in plasmonic devices," Plasmonics **15**, 2137 (2020).
51. S. Kim, S. Lepeshov, A. Krasnok, *et al.*, "Beyond bounds on light scattering with complex frequency excitations," Phys. Rev. Lett. **129**, 203601 (2022).
52. K. Tsakmakidis, T. Pickering, J. Hamm, *et al.*, "Completely stopped and dispersionless light in plasmonic waveguides," Phys. Rev. Lett. **112**, 167401 (2014).
53. F. Guan, X. Guo, K. Zeng, *et al.*, "Overcoming losses in superlenses with synthetic waves of complex frequency," Science **381**, 766 (2023).
54. F. Guan, X. Guo, S. Zhang, *et al.*, "Compensating losses in polariton propagation with synthesized complex frequency excitation," Nat. Mater. **23**, 506 (2024).
55. K. Zeng, C. Wu, X. Guo, *et al.*, "Synthesized complex-frequency excitation for ultrasensitive molecular sensing," eLight **4**, 1 (2024).
56. Q. Cheng and T. Li, "Complex-frequency waves: beat loss and win sensitivity," Light Sci. Appl. **13**, 40 (2024).
57. HITRAN, "High-resolution transmission molecular absorption database," (2014). https://hitran.org.